Acta Biomaterialia 44 (2016) 209–220

Contents lists available at ScienceDirect

Acta Biomaterialia

journal homepage: www.elsevier.com/locate/actabiomat

Full length article

Natural myocardial ECM patch drives cardiac progenitor based restoration even after scarring

Udi Sarig PhD [a,1], Hadar Sarig PhD [a,1], Elio de-Berardinis MSc [a], Su-Yin Chaw MSc [a], Evelyne B.V. Nguyen PhD [a], Vaibavi S. Ramanujam MSc [b], Vu D. Thang MD [b], Muthafar Al-Haddawi DVSc, PhD, Dip. ACVP [c], Susan Liao PhD [a], Dror Seliktar PhD [b,d], Theodoros Kofidis MD, PhD [b], Freddy Y.C. Boey PhD [a], Subbu S. Venkatraman PhD [a,*], Marcelle Machluf PhD [a,e,*]

[a] School of Materials and Science Engineering, Nanyang Technological University, Singapore 639798, Singapore
[b] Yong Loo Lin School of Medicine, National University of Singapore, Singapore 119228, Singapore
[c] Institute of Molecular and Cell Biology, Agency for Science, Technology and Research, Singapore 138673, Singapore
[d] Faculty of Biomedical Engineering, Technion – Israel Institute of Technology, Haifa 32000, Israel
[e] Faculty of Biotechnology and Food Engineering, Technion – Israel Institute of Technology, Haifa 32000, Israel

ARTICLE INFO

Article history:
Received 28 March 2016
Received in revised form 16 August 2016
Accepted 17 August 2016
Available online 18 August 2016

Keywords:
Myocardial infarction
Heart regeneration
Extracellular matrix
Tissue engineering
Cardiac progenitors
Bioactive patch

ABSTRACT

Objective: To evaluate the regenerative capacity of *non-supplemented and bioactive patches* made of decellularized porcine cardiac extracellular matrix (pcECM) and characterize the biological key factors involved in possible cardiac function (CF) restoration following acute and 8 weeks chronic MI.
Background: pcECM is a key natural biomaterial that can affect cardiac regeneration following myocardial infarction (MI), through mechanisms, which are still not clearly understood.
Methods: Wistar rats underwent MI and received pcECM patch (pcECM-P) treatment in either acute or chronic inflammatory phases. Treated, sham operated (no MI), and control (MI without treatment) animals, were compared through echocardiography, hemodynamics, pathological evaluation and analyses of various mRNA and protein level markers.
Results: Our results show that in both acute and long-term chronic MI models, pcECM promotes significant cardiac function improvement, which is correlated to progenitor ($GATA4^+$, c-kit^+) and myocyte ($MYLC^+$, $TRPI^+$) recruitment. Interestingly, recruited progenitors, isolated using laser capture microdissection (LCM), expressed both early and late cardiomyocyte (CM) differentiation markers, suggesting differentiation towards the CM lineage. Recruited CM-like cells organized in a partially striated and immature muscle fiber arrangement that presented connexin43 —a crucial mediator of cardiac electrical conductivity. Concomitantly, pcECM was rapidly vascularized, and induced a constructive remodeling process as indicated by increased M2/M1 macrophage phenotypic ratio and pathological evaluation.
Conclusions: Acellular pcECM patch implants alone, i.e., without added biologics, are bioactive, and exert potent efficacy, stimulating biological regenerative processes that cooperatively lead to *a cardiac progenitor-based restoration of function*, even after scar tissue had already formed.

Statement of Significance

MI ('heart attack') remains the leading cause of heart failure and death in developed-countries. Restoration of cardiac function requires active turnover of damaged heart contracting cells (CM), however, CM endogenous regeneration is not efficient and is a matter of controversy. We show that a bioactive biomaterial alone—decellularized heart tissue (pcECM)—without added cells or growth factors, can elicit a complex regenerative response even after irreversible scarring. The pcECM patch induces macrophage polarization towards constructive remodeling and cardiomyocyte progenitor cell ($GATA4^+$, c-kit^+) recruitment (evidenced at both mRNA and protein levels) resulting in *de novo*

* Corresponding authors at: The Laboratory of Cancer Drug Delivery & Mammalian Cell Technology, Faculty of Biotechnology & Food Engineering, Technion – Israel Institute of Technology, Haifa 32000, Israel (M. Machluf), School of Materials Science and Engineering, Nanyang Technological University, 50 Nanyang Avenue, Singapore 639798, Singapore (S.S. Venkatraman).
E-mail addresses: assubbu@ntu.edu.sg (S.S. Venkatraman), machlufm@tx.technion.ac.il (M. Machluf).
[1] These authors contributed equally to this paper.

http://dx.doi.org/10.1016/j.actbio.2016.08.031
1742-7061/

immature striated-like muscle patterns (MLC$^+$, TrpI$^+$, connexin43$^+$). We, therefore, suggest this bioactive pcECM can model cardiac regeneration, and serve as a candidate for fast-track clinical application.

1. Introduction

The ideal therapy for myocardial infarction (MI) needs to biologically stimulate and induce regeneration, address cardiac mechanics, and consider the inflammatory stage of infarct scarring during intervention. Biomaterials, of synthetic (e.g., PU, PLGA) and natural (e.g., alginate, collagen, fibrin) origin, in either a patch or injectable treatment modality, are widely suggested treatments for the infarcted myocardium, each having its own pros and cons as comprehensively reviewed elsewhere [1–3]. Typically, biomaterial-treatments provide passive physical support to the infarcted ventricle, preventing further deterioration according to the modified law of Laplace [4]. Biological stimulation, however, is essential for restoration of cardiac function (CF), and is mediated by either bioactive factors incorporation into the biomaterials, and/or through other intrinsic bio-inductive scaffold characteristics. While biologics incorporation, e.g., cells, progenitor recruiting cytokines and growth factors [2,5,6], has been previously suggested for MI treatment, several major hurdles inhibit progress in the experimental and regulatory route to effective translation of this approach. As tissue repair mechanisms remain complex and are not yet fully known, defining the optimal composition, sources and desirable release profiles of the biologics needed to reach an ideal regenerative response remains challenging. Second, with each biologic agent affecting a spectrum of biochemical pathways, the implications of any such myriad combination is difficult to predict, and can be expected to increase the burden and complexity of the associated regulation. Alternatively, a promising class of intrinsically bio-inductive biomaterials is decellularized extracellular matrices (ECM), whose major advantage lies in their high bioactivity i.e., their ability to stimulate cell recruitment, attachment, survival, proliferation, migration, and differentiation [7]. Moreover, ECM's reciprocal cross-talk with its resident cells can affect numerous regenerative and reparative processes [8,9].

In cardiac therapy, ECMs of non-myocardial tissues were previously suggested as adequate biomaterials for cardiac augmentation [10–13]; however, as ECM differ from one tissue to another, they may intrinsically lack the optimal composition, ultrastructure, biomechanical and biochemical cues that constitute a prerequisite for myocardial-specific support and regeneration [3,14,15]. Several myocardial ECM scaffolds were isolated from rat [16,17], porcine [18–22] and human [23,24] origin. In particular, porcine cardiac derived ECM (pcECM) displayed promising cell support ability [20,25], myocardial matching mechanical properties [20,22,26], and human equivalent composition [20,22]. In addition, pcECM availability and reproducibility can be assured through stringent quality control, suggesting xenograft clinical relevancy [2,16,18,22,24]. Nevertheless, the ability of pcECM to induce a myocardial reparative process and its possible biological mediators remain largely unknown, especially in chronic MI models, which are characterized by the presence of a mature and irreversible scar tissue prior to treatment administration.

Accordingly, we hypothesize that natural, bioactive and non-supplemented acellular pcECM patches (pcECM-P) can improve CF, even after scarring, and increase contractility through biological mechanism of action. The role of pcECM-P in restoration of CF was studied herein in both acute and chronic MI models, i.e., before and after scar tissue formation, respectively. Cardiac energetics, dimensional, and functional parameters were monitored through echocardiography and hemodynamics. By implanting acellular pcECM-P, we were able to explant and study the involvement of various recruited cell types, including progenitors, at the mRNA and protein level expression of various cardiac, vascular, and innate immunity markers. Based on our experimental data we suggest a biological, model-independent mechanism that explains the potent pcECM-P efficacy reported herein. We further suggest that a pcECM patch treatment can provide an important platform for mechanistic studies of ECM bioactivity and a good candidate for future fast-track clinical applications.

2. Materials and methods

2.1. Experimental design

All procedures and animal handling were approved and performed in accordance to Institutional Animal Care and Use Committee (IACUC) guidelines, National University of Singapore. A total of 88 male Wistar Rats (300–350 g), were randomly divided into eleven groups defined by their sacrifice time point and their treatment modality (n = 8 rats per group and time point, Supplementary Table S1). Two MI models were studied – an acute model, in which treatment was given immediately after MI induction; and a chronic model, in which two surgeries were performed—the first for MI induction and the second, 30 days afterwards, for treatment. For all experiments, pcECM matrices were randomly distributed between groups. Each model had its own control and sham operation groups (positive control) as indicated in Supplementary Table S1. All controls underwent MI and suturing similarly to patch attachment just without the pcECM to rule out possible recovery effect due to stunned myocardium. All animals were monitored by echocardiography throughout the experimental timeline; at end-points, evaluation was through invasive hemodynamic assessment and a thorough double-blinded pathological investigation. For isolation of recruited cells' mRNA, five additional rats were treated with pcECM-P in an acute model and allocated for careful patch isolation using laser capture microdissection (LCM), 30 days post implantation. The extracted mRNA was studied by qPCR for the expression of 14 representative CM early and late developmental markers, and compared to neonatal rat CM and mature rat heart samples as controls. To better understand the organization and contribution of particular recruited cell population subsets at the protein level, selected markers of cardiac, vascular and innate immunity were visualized, quantified, and studied for their possible correlation to functional improvements using immunohistochemistry (IHC) and immunofluorescent (IF) stains.

2.2. Implant preparation

Acellular pcECM (1.5 cm diameter, 1.5 mm thick) patches were produced and disinfected as previously published [20]. Briefly, female pig (40–70Kg) hearts were harvested in cold sterile PBS containing 200U/ml penicillin, 0.2 mg/ml streptomycin (Pen-Strep, Biological Industries) and 2 μg/ml amphotericin B (Fungizone®, Gibco). Left ventricles were isolated and horizontally cut in three. The two larger rings were further cut longitudinally into 3–4 parts, which were sliced parallel to the epicardial plain into 3 mm thick sections. The myocardial tissue sections were

sequentially washed in hypertonic (1.1% NaCl – 0.02% EDTA, Sigma) and hypotonic (0.7% NaCl – 0.02% EDTA) solutions for two hours each, followed by immersion in 0.05% Trypsin (Sigma) – 0.02% EDTA in PBS at pH 7.4 and 37 °C (supplemented with Pen-Strep and Fungizone) for two 24 h cycles. Finally, treated slices were agitated in a fresh detergent solution of 1% Triton®-X-100 (Ethylene glycol octyl phenyl ether) and 0.1% ammonium hydroxide in PBS for four consecutive 48 h cycles, and extensively washed in DDW to remove any detergent remains. Effective decellularization was evaluated by whitening of the patch material and verified by picogreen DNA quantification as well as histological cross sectional stains for Masson trichrome and H&E (data not shown). Prior to implantation, 70%(v/v) ethanol disinfected patches were washed with PBS containing double antibiotic concentration (Pen-Strep and Fungizone), followed by immersion in standard culture media (standard αMEM, Biological Industries with antibiotics but without serum) for 1–2 h at 37 °C and in 5% CO_2.

2.3. Induction of MI and pcECM treatment

Male Wistar rats were anesthetized using a 3–5% isoflurane/oxygen mixture, intubated and mechanically ventilated (Inspira ASV ventilator, Harvard Apparatus, Holliston, MA). The heart was exposed by left thoracotomy and pericardiectomy via the 5th intercostal space. The left anterior descending (LAD) coronary artery was ligated proximally using a 7–0 Premilene® suture (B. Braun, Aesculap, Tuttlingen, Germany). Infarction was confirmed by visible blanching of the left ventricle (LV) and significant ECG changes. pcECM-Ps were sutured (7/0 absorbable glyconate suture, Monosync, B. Braun) onto the infarcted area either immediately (acute) or 30 days (chronic) post MI, as indicated. To assess the suturing effect, additional n = 8 rats received patch gluing without sutures (TISSEEL fibrin sealant, Baxter, UK; Supplementary Fig. S1) and were monitored through echocardiography for 30 days. Control animals did not receive any treatment after MI induction, apart from sham sutures to rule out stunned myocardial recovery; while sham group animals underwent only thoracotomy and pericardiectomy. Following chest closure in layers and extubation, animals were transferred to an intensive care unit for recovery and received subcutaneous administration of Enrofloxacin (25 mg/kg) and Buprenorphine (0.05 mg/kg) for up to 5 days.

2.4. Echocardiography

Transthoracic echocardiography was performed under general anesthesia before MI induction (i.e., baseline reads) and at specified time points postoperatively, using the Vivid S6 ultrasound system (General Electric VingMed, Horton, Norway) equipped with a i12L-RS linear array transducer (5–13 MHz). Acquired B- (Brightness, 2D) and M- (Motion) mode images and data were analyzed by EchoPac™ software (Version 6.0, General Electric Vingmed, Horten, Norway). Functional parameters monitored were ejection fraction (%EF), fractional area change (%FAC) and fractional shortening (%FS). Dimensional parameters monitored were: left ventricle interior diameter in diastole and systole (LVIDd and LVIDs, respectively), inter-ventricular septum dimension in diastole and systole (IVSd and IVSs, respectively) and left ventricle posterior wall dimension in diastole and systole (LVPWd and LVPWs, respectively). Relative infarct size was determined only at diastole (to minimize measurement error) as the percentage of the akinetic region to the entire left ventricular circumference, averaged from three consecutive samples at the papillary muscle level in the short axis view, based on a previously published methodology [27,28]. All other formulas used for calculations of echocardiographic data were as previously established [29] and detailed in Supplementary Table S2. To avoid random block effect in any particular parameter monitored, all dimensional data results presented are an average ± SD of paired baseline normalized values. That is, for each rat the 30 days post pcECM-P implantation dimensional value was normalized to its own baseline value (measured prior to infarction for LVID, LVPW and IVS; or 3 days post infarction for Infarct size and the normalized values were averaged per group.

2.5. Hemodynamic analysis

Hemodynamic assessments were performed immediately prior to sacrifice as previously published [30]. Briefly, following median sternotomy, a 2 mm transit-time flow probe (Transonic Systems, Ithaca, NY, USA) was placed around the ascending aorta for cardiac output measurement used for volume calibration (α calibration). A pressure–volume (P-V) catheter (SPR-838 NR, Millar Instruments, Houston, TX) was inserted into the left ventricle for left ventricular pressure–volume relation studies, using the MPVS-Ultra system (Millar Instruments, Houston, TX) and PowerLab 16/30 (AD Instruments, Mountain View, CA). Volume calibration was performed using the 910–1048 vol Calibration Cuvette (2–15 mm wells) (AD Instruments, Mountain View, CA), according to the manufacturer's instructions. A saline calibration (50–100 μl of 30% w/v NaCl in DDW) was used to determine parallel volume (V_p).

Cardiac dimensional and functional characteristic parameters were obtained from analyses and calculations using LabchartPro™ software (AD Instruments, Mountain View, CA) of at least five consecutive cardiac cycles within baseline normal recordings. These included maximal and mean pressures per cycle (P_{max} and P_{mean}, respectively), end diastolic/systolic pressures and volumes (EDP, ESP and EDV, ESV, respectively), cardiac output [CO = (EDV − ESV)*heart rate], stroke work (SW, area blocked within the P-V loop), maximal slopes of systolic and diastolic pressure ($+dP/dt_{max}$ and $-dP/dt_{min}$), time constants of LV pressure decay (Tau) and the average -dp/dt during the diastole isovolumetric relaxation periods (IRP average dp/dt).

Inferior vena cava occlusion tests were performed to assess preload independent LV parameters: maximal ventricular elastance ($E_{es/max}$, measured as the slope of the ESP volume relationship linear curve, ESPVR); slope of the EDP volume relationship (EDPVR) linear curve; preload recruitable stroke work (PRSW, measured as the slope of the SW to ESV linear fitting curve); pressure volume area (PVA), which marks the blocked area between the EDPVR, the ESPVR and the systolic curve of the PV loop under normal conditions at the beginning of the occlusion test (equals the total energy generated by the ventricular contraction), and cardiac efficiency (defined as the ratio of SW/PVA). Representative PV loops of baseline and occlusion tests for normal (sham) hearts, MI controls and pcECM-P treated hearts in acute and chronic models are presented in Supplementary Fig. S2.

2.6. Histopathological assessment

Following hemodynamic recordings, animals were euthanized. Necropsies were performed on three randomly selected animals from each treatment group. During necropsy, major organs (lungs, liver, spleen, brain, kidneys, tracheal and bronchial lymph nodes) were extracted and pathologically inspected for gross pathological findings, followed by organ fixation in neutral buffered formalin (NBF, 10%v/v, Sigma, St. Louis, MO) at room temperature. For cardiac assessment, all hearts were transversely cut in the middle of both ventricles through the infarct zone (with/without the patch) in the LV. Both sections were processed to paraffin blocks, sectioned (5 μm, Leica RM2255/ RM2235 Microtome, Germany) and stained with hematoxylin and eosin (H&E, Richard-Allan Scientific™, Thermo Scientific, MA). A double-blinded evaluation and lesion scoring of histopathology slides were performed (on at least

three sections per animal per staining) by a Board certified veterinary pathologist (MAH). Scoring was performed using quantitative criteria for features of inflammatory and tissue remodeling response after implantation of decellularized scaffold materials, as previously described [31], and detailed in Supplementary Table S3. Higher scores are indicative of a constructive remodeling response whereas low scores are indicative of scar tissue or foreign body type response. Following blinded scoring, animal attribution was revealed to enable concluding pathological remarks per group. Sequential sections were also stained by Masson's trichrome (MTC) as previously published [32] to evaluate patch and infarct locations, morphology and dimensions (identified by the blue color staining).

2.7. LCM, mRNA isolation and analyses

Randomly assigned hearts (n = 5 hearts) were harvested 30 days post implantation of pcECM-P in an acute model. Hearts were quickly rinsed in PBS, snap-frozen in liquid nitrogen, and stored at −80 °C until sectioning. Ten μm cross-sections (without OCT embedding) were cut (Leica CS5030 cryostat, Germany) and mounted on PEN membrane slides (Life Technologies, CA). LCM of patch areas only (Arcturus LCM, Life Technologies, CA) was performed according to the manufacturer's instructions using CapSure® Macro Caps (Life Technologies, CA). Patch areas were manually determined, leaving a safe distance from the infarct-patch interface, and the dissected areas were imaged prior to and following dissection to ensure no contaminating mRNA from the infarct or heart were accidentally collected. RNA was extracted separately from each heart sections' pool (at least 4 patch sections per sample) using the PicoPure RNA isolation kit® (Life Technologies, CA). Neonatal rat CM (Lonza, Switzerland) and native heart tissue (n ⩾ 3 for each sample type) were processed for mRNA isolation using QIAzol Lysis reagent and miRNeasy mini Kit (Qiagen, Netherlands). All mRNA samples were subsequently evaluated by qPCR (BioRad CFX96 analyzer, BioRad, CA) with custom designed (Supplementary Table S4) short amplicons (~70–80 bp) using the Exiqon LNA™ system (Exiqon, Denmark) and relevant syber-green based amplification reagents (ScienceWerke, Singapore). All data pre-processing and analyses were performed using GenEx 6.0.3.415 (MultiD, Sweden) for interplate calibration, data validation, automatic imputation housekeeping gene normalization, technical replicates averaging (n = 3 technical run per biological replica), logarithmic transformation, autoscaling and analyses. The analyses included principal components analyses (PCA), and Ward's method clustering based on absolute Pearson's correlation for genes and samples (generating gene expression relative 'heat maps').

2.8. Immunohistochemical (IHC) and immunofluorescent (IF) assessments

IHC staining was performed using several primary antibodies evaluating various aspects of pcECM bio-activity, integration and compatibility. Primary antibodies used: rabbit anti-rat GATA4, MYLC, c-kit, connexin43, von-willebrand factor (vWF) and CCR7 (Abcam, Cambridge, UK); rabbit anti-rat CD31; goat anti-rat CD206 (Santacruz Biotechnology, Dallas, TX) and vimentin (Millipore); and mouse anti-rat α-smooth muscle actin (α-SMA, CellMarque, Rocklin, CA), MYLC and Troponin I (Abcam, UK). IHC stains were performed automatically according to the manufacturer's instructions (Leica Bond™ autostainers, Leica Microsystems, Germany). Immunofluorescet (IF) stains were manually performed. Each section was pre-treated with Image-iT™ FX (Life Technologies) signal enhancer for 30 min at room temperature, blocked with 5% donkey serum and stained with sequential (1st primary → 1st secondary → 2nd primary → 2nd secondary) antibody incubations at room temperature. All antibody dilutions and washing (3 washes after each incubation step) were in blocking solution comprising 5% donkey serum. Primary antibodies were incubated for 60 min and secondary antibodies—for 30 min, followed by DAPI counter staining (NucBlue®, Life Technologies), mounting (ImmuMount™, Thermo Scientific) and nail-polish sealing. Image acquisition was performed using a Nikon eclipse TE2000 inverted microscope. Supplementary Table S5 summarizes the appropriate dilutions and staining conditions for both IHC and IF.

2.9. Image analyses and quantifications

Histological and IHC stains' image analyses were performed by manual annotation of at least seven random squares (minimum 0.2 mm^2 per square) in distinct regions of patch, infarct and their interface. Positive cells and blood vessel quantity were independently and blindly counted by three persons and normalized to surface area. Representative pictures of at least three technical repeated sections for each animal (n ⩾ 3 animals that were IHC analyzed per group per time point and antibody staining) are presented.

2.10. Statistical analyses

Sample size was a priori determined based on a statistical power of 95% (for k = 3 sample means), at conventional $\alpha = 0.05$, as evaluated from previously published data of similar acute rat models [33]. Outliers, if present, were excluded based on the mahalanobis D^2 method. All results were found to be normally distributed according to the Shapiro-Wilk goodness of fit W test. Results are expressed as the mean ± standard deviation of each group. Statistical significance was evaluated by one-way analyses of variance (ANOVA) and Tukey's HSD test for multiple comparisons at individual time-point experiments, and by two-way ANOVA with post hoc corrections for time and model comparisons when applicable, using JMP 6.0 statistical software (SAS™, Cary, NC). For all comparisons, $p < 0.05$ was considered significant. Assay specific sample size and additional statistical analyses methods are mentioned in the relevant methodology sections of the supplemental online data.

For comparison purposes, unless otherwise stated, data are presented for the 30-day time-points post implantation, i.e., 30 and 60 days post MI for the acute and chronic models, respectively, accompanied by a corresponding control group.

3. Results

Initial infarction size was similar between groups (26 ± 9%, Supplementary Fig. S3).

3.1. Echocardiographic assessment

Significant improvements of the left ventricle (LV) systolic and diastolic dimensions were observed 30 days post treatment (Fig. 1). In both models, pcECM-P significantly reduced the normalized infarct size, and left ventricular internal diameter (LVID), while increasing the left ventricular posterior wall thickness (LVWP) towards the sham values. The systolic thickness of the inter-ventricular septum (IVS)—signifying the compensatory response of the healthy myocardium to infarction—in the treated groups was similar to the sham and significantly higher than the control in both models. In general, apart from relative infarct size (quantified only in diastole), all other parameters exhibited higher change-amplitude in systole compared to diastole.

Concomitantly, in both models dramatic functional improvements ($p < 0.001$) were observed in fractional area change (FAC), ejection fraction (EF) and fractional shortening (FS) towards the 'normal' sham values, when compared to the non-treated controls (Fig. 2). In the acute model, the average FAC at 60 days post treatment was even similar to the sham group value (Fig. 2A). Similar observations were obtained for patches glued on top of the infarcts (instead of sutures, Supplementary Fig. S1), demonstrating patch efficacy that is independent of the implantation method.

3.2. Hemodynamic assessment

Under normal baseline recordings, pcECM-P treated hearts in both models graphically displayed P-V loops, which approximated sham appearance (Supplementary Fig. S2), as also reflected in significantly higher generated pressures and cardiac outputs (Supplementary Table S6). Furthermore, the patch-treated groups displayed restoration in most baseline parameters (Fig. 3A-E to levels similar to the sham group ($p > 0.05$).

Preload independent hemodynamic measurements taken during occlusion tests (Fig. 3F–H) provided similar findings in both models. The differences between treatment and control groups were graphically apparent by the slope of the end systolic pressure volume relationship (ESPVR) curve (Supplementary Fig. S2)—representing the maximal cardiac elastance (E_{es}, Fig. 3F). Parallel significant salvage was observed in terms of heart efficiency, and preload recruitable stroke work (PRSW, Fig. 3G-H, respectively) for both acute and chronic models.

3.3. Pathological evaluation

Patches remained attached to treated hearts, and were mildly degraded (still largely intact even 60 days post implantation), with lack of connective-tissue disruption, slight to no-encapsulation, and no apparent multinucleated giant cells (Fig. 4). Similar levels of infiltrating cells appeared in the patch–infarct interface and within the core of the patch, in both models.

Pathological scoring indicated the pcECM biocompatibility and its induction of a constructive remodeling process (Supplementary Table S3), based on previously established criteria [31]. Macrophage quantification of the M2/M1 ratio in the acute model, revealed a time-dependent increase up to 60 days post implantation (Fig. 5). Similar ratios were measured in both models, 30 days post treatment (Fig. 5C), which were also comparable to their equivalent untreated control values (1.2 ± 0.6, $p > 0.05$, data not shown).

CD31, vWF and α-SMA stains were used to evaluate the mean vessel density (MVD) in both infarct and patch areas. MVD levels within the infarcts of both treated and control groups remained the same for all time-points in both models ($p > 0.05$, 65 ± 35 vessels/mm^2, data not shown). In comparison, MVDs within the pcECM-Ps were significantly higher 14 days post treatment and gradually decreased over time, being still significant at 30 days and reaching values that are similar to baseline at 60 days (Fig. 6). The vascularity of the pcECM-P in both models, 30 days post implantation, was similar ($p > 0.05$) and appeared to be denser closer to the interface with the host.

3.4. Recruitment of cardiac progenitor and muscle cells

pcECM-Ps were carefully isolated from the explanted infarcted ventricles of the acute model 30 days post implantation using LCM (Fig. 7A). Principal component analyses (PCA) positioned the mRNA expression profile of pcECM-P-recruited cells between that of rat neonatal CM (NRCM) and mature rat heart (MRH, Fig. 7B, 'scores'). All cardiomyocyte markers studied were positively

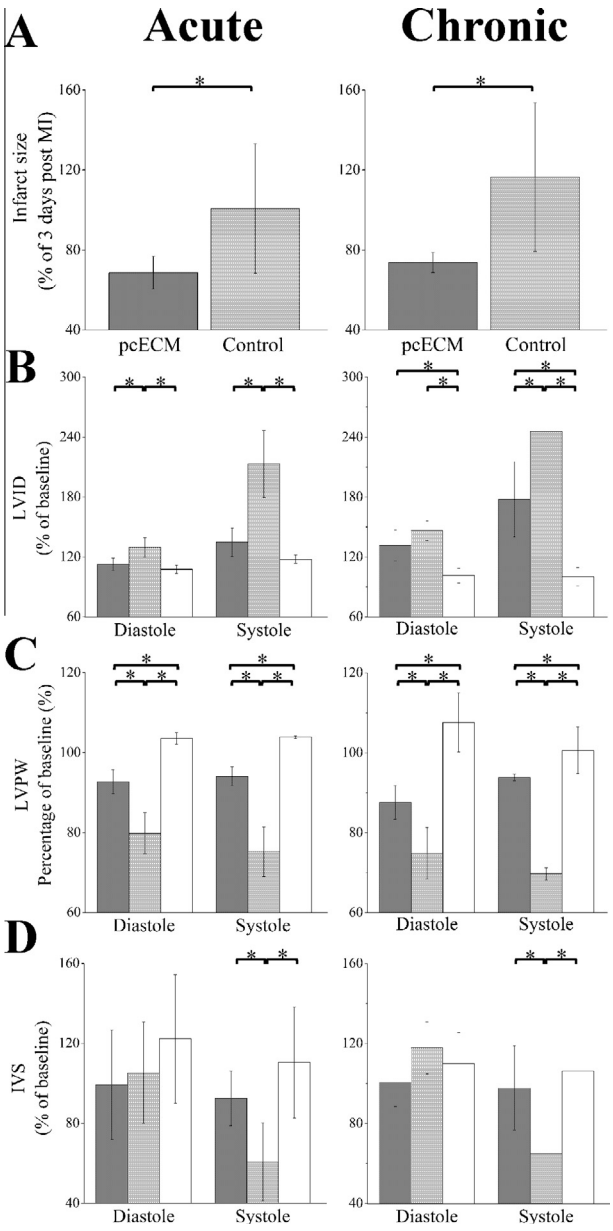

Fig. 1. Echocardiography evaluation of cardiac dimensions 30 days post treatment for acute and chronic models (left and right panels, respectively). Relative infarct size (A, normalized to the value at 3 days post infarction), LV internal diameter (LVID), LV posterior wall thickness (LVPW), and inter-ventricular septum thickness (IVS) (B-D, respectively, normalized to baseline values). Dark gray—pcECM-treated group; Light gray—control; white—sham. *Statistical significance indicator ($p < 0.05$). Results represent the mean ± SD of each group as indicated in Supplementary Table S1.

expressed within the isolated pcECM-P samples, and were generally clustered into two groups indicating the major contributors to the progenitor/neonatal vs. the mature states (Fig. 7B 'loadings'). These findings were also confirmed by independent heat-map clustering (Fig. 7C).

Representative 'progenitor' (GATA4 and c-kit (KIT)) and 'mature' (MYLC and TrpI) markers were further evaluated at the protein level (Fig. 8A-B). Image analysis quantification (Fig. 8C-F) revealed that only GATA4$^+$ and MYLC$^+$ cell densities significantly increased through time (Fig. 8C-D, respectively) displaying linear penetration rates ($R^2 > 0.95$, Supplementary Fig. S4). The ratio between GATA4$^+$/MYLC$^+$ cells, however, declined logarithmically over time, stabilizing at a 5:1 ratio beyond the 30-day

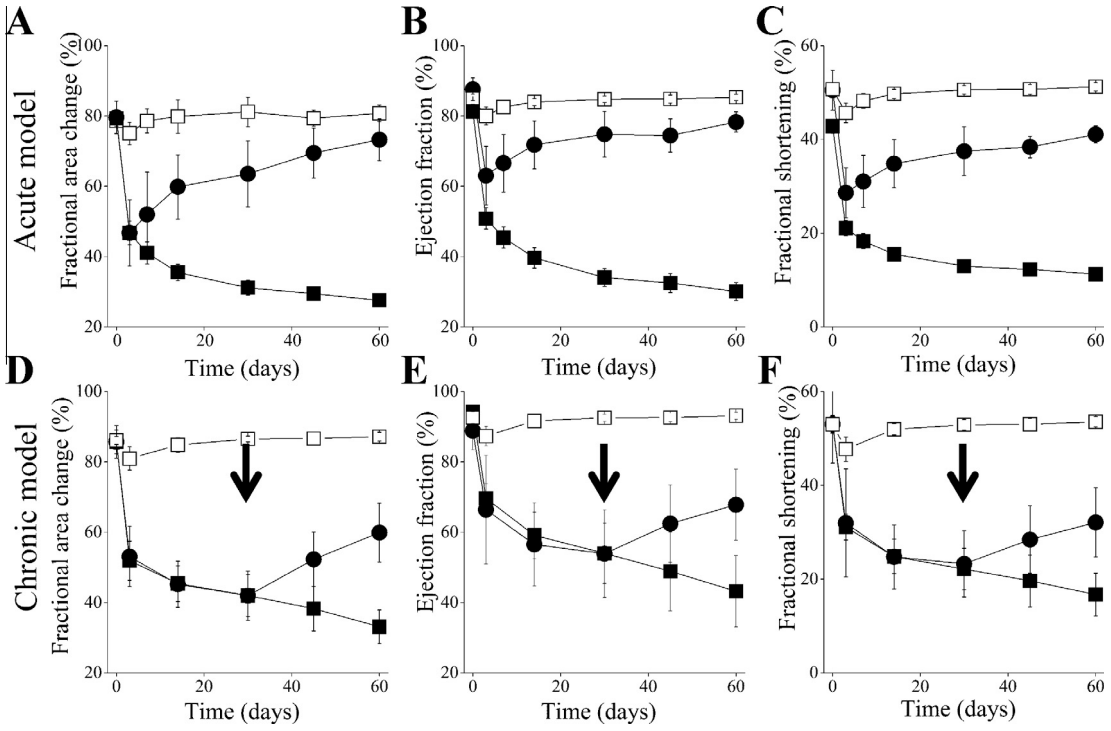

Fig. 2. Echocardiographic evaluation of CF and it correlation to progenitor and muscle cell recruitment. Fractional area change (FAC), ejection fraction (EF) and fractional shortening (FS) kinetics in acute (A–C, respectively) and chronic (D–F, respectively) models. Symbols: Open squares—sham; circles—pcECM-P treated group; closed squares—control. Arrows indicate the treatment time-point. Results represent the mean ± SD of each group and time point as indicated in Supplementary Table S1.

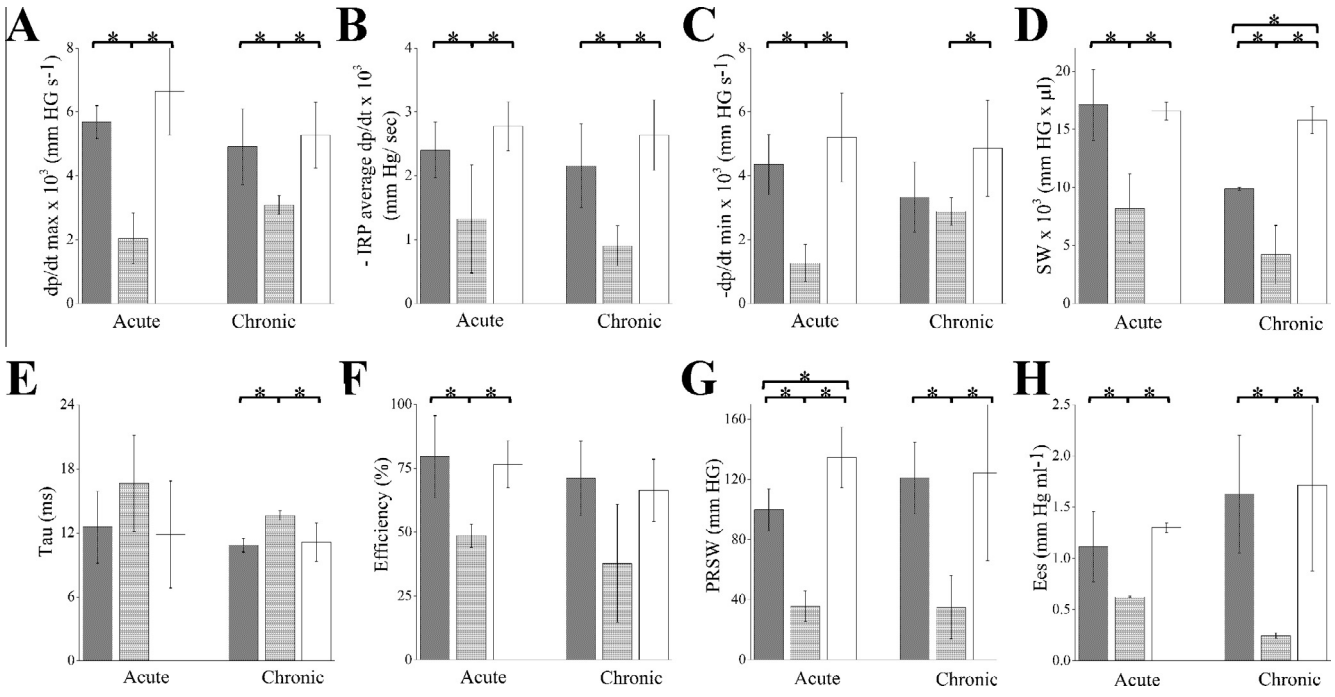

Fig. 3. Hemodynamic evaluation of cardiac function and contractility 30 days post treatment. Parameters measured under physiological normal conditions: Peak rate of pressure rise (dp/dt_{max}, A), average pressure decline during isovolumetric relaxation period (−IRP average dp/dt, B), peak rate of pressure decline ($-dp/dt_{min}$, C), and Stroke work (SW, D). Parameters measured during occlusion tests: Cardiac end systolic elastance (E_{es}, *E*), cardiac efficiency (F), preload recruitable stroke work (PRSW, G) and relaxation time constant calculated by Weiss method (Tau, H). Dark gray—pcECM treated group; light gray—control; white—sham. *Statistical significance indicator ($p < 0.05$). Results represent the mean ± SD of each group as indicated in Supplementary Table S1.

time-point. Interestingly, the effect of time was not significant for c-kit$^+$ (Fig. 8E), total (Fig. 8F) or TrpI$^+$ (data not shown) cells. Moreover, quantified GATA4$^+$ and MYLC$^+$ cell densities within the patch were highly correlated to FS as a representative functional parameter ($R^2 = 0.888$ and 0.635, respectively) (Fig. 8C and Fig. 8D, respectively). No correlation to functional improvement was observed, however, in the case of c-kit$^+$ (Fig. 8E), total cell quantities (Fig. 8F) or TrpI$^+$ cells (data not shown).

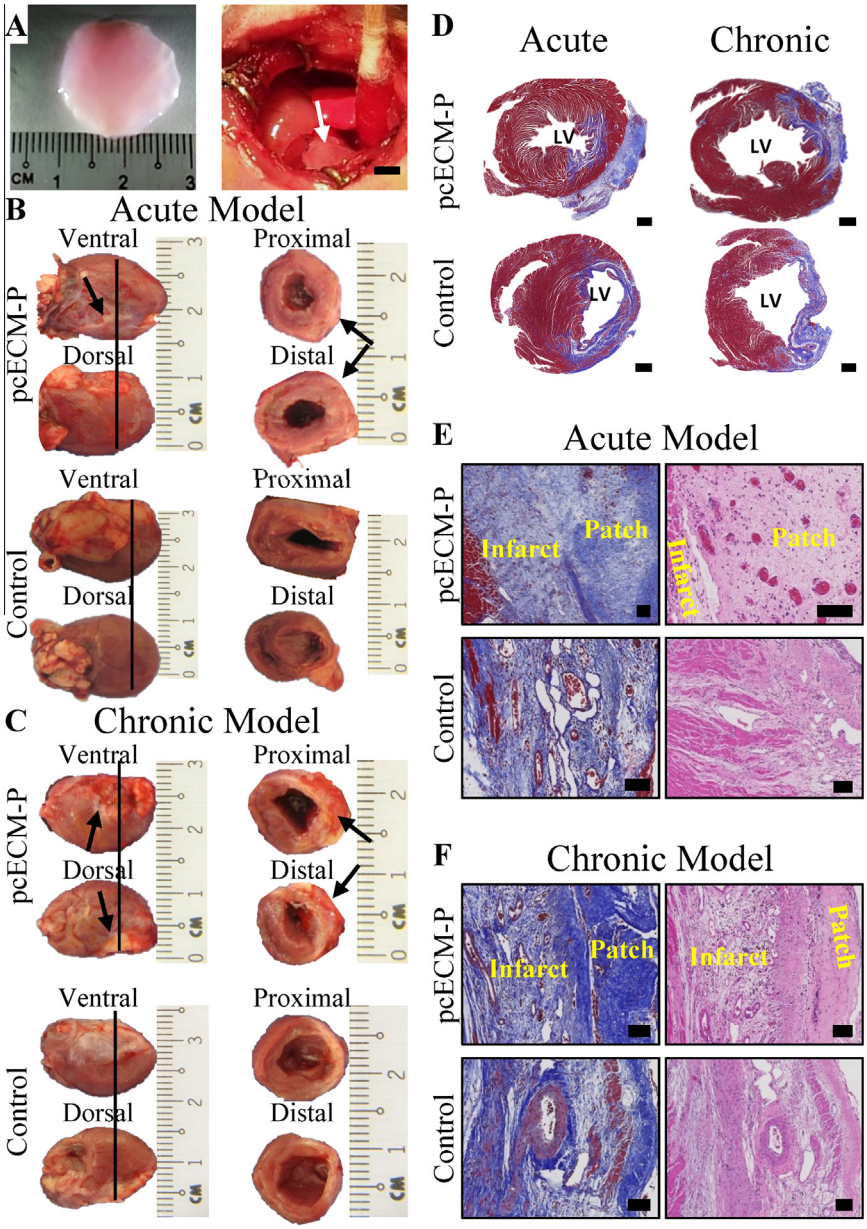

Fig. 4. PcECM-P implantation and microscopic evaluation. pcECM-P is soaked in normal culture media (A, left) and sutured onto infarcted rat heart (A, right). Representative gross pictures of explanted pcECM-P treated hearts 30 days post implantation in acute (B) and chronic (C) models are shown next to their respective controls, as indicated; arrows point to patch area. Vertical black lines (B and C, left) mark the cutting planes on ventral and dorsal views to enable the proximal and distal cross sectional views on the right. Representative overview images of left ventricular (LV) Masson's Tri-Chrome (MTC) stains for patch treated hearts 30 days post implantation in acute and chronic models next to their respective non-treated MI controls (D). Higher magnifications of MTC (left) and Hematoxylin and Eosin (H&E, right) stains in both acute (*E*) and chronic (F) models. Scale bars: (A, right)–5 mm; (D)–1 mm; (*E* – F)–100 μm.

MYLC organized within the cytoplasm of what appeared to be incomplete *de novo* fiber-like morphology of CM-like ($MYLC^+$) cells ensheathed by fibroblastic cells ($Vimentin^+$, Fig. 8G). In some cases, partially striated muscle-like fibers appeared to form within the patch (Supplementary Fig. S5). GATA4 and the cardiac specific gap–junctional protein—Connexin43—were co-localized within the $MYLC^+$ cells recruited to the patch. However, while c-kit was readily visualized within some cells at the patch area, not all $c\text{-}kit^+$ cells were co-localized with GATA4 (Fig. 8G).

4. Discussion

Most studies to date, utilized myocardial ECM for cardiac repair in its injectable form—produced through harsh ECM grinding, and acidic and enzymatic digestion—suggesting its possible biological activity, through mechanisms, which are still not clearly understood [18]. This limited mechanistic understanding may result from the complexity in pinpointing the *injectable* ECM role in the remodeling process as, unlike the patch, it cannot be easily retrieved from the infarcted tissue. pcECM *patches*, on the other hand, preserve their original, unaltered and bioactive natural morphology and composition, while displaying superior ventricular mechanical support.

Our results clearly indicate that pcECM-P is able to not only prevent further deterioration in *both acute and chronic MI models*, but also improve contractility, ventricular dimensions and cardiac remodeling. In particular, FAC, ESPVR slope (Ees), dp/dt_{max} and cardiac efficiency even achieved normal-like values with time. As

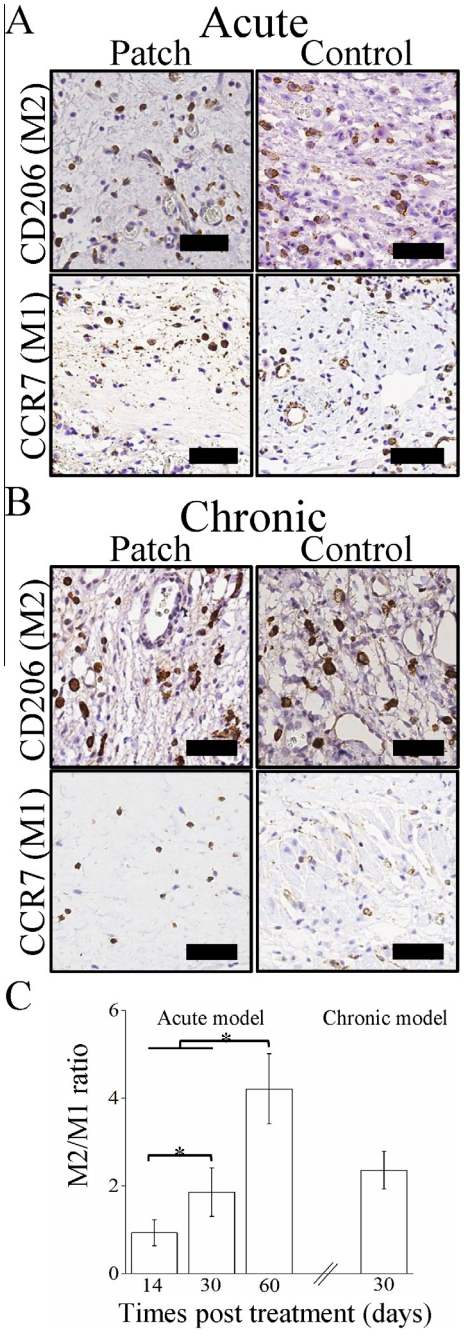

Fig. 5. pcECM-P induces favorable macrophage polarization. M2 and M1 representative IHC stains for acute (A) and chronic (B) models 30 days post treatment. M2/M1 ratio quantification (mean ± SD of n = 6 animals per time point) for 14, 30 and 60 (acute) and 30 (chronic) days post treatment (C). *Statistical significance indicator ($p < 0.05$). Scale bars: 50 μm.

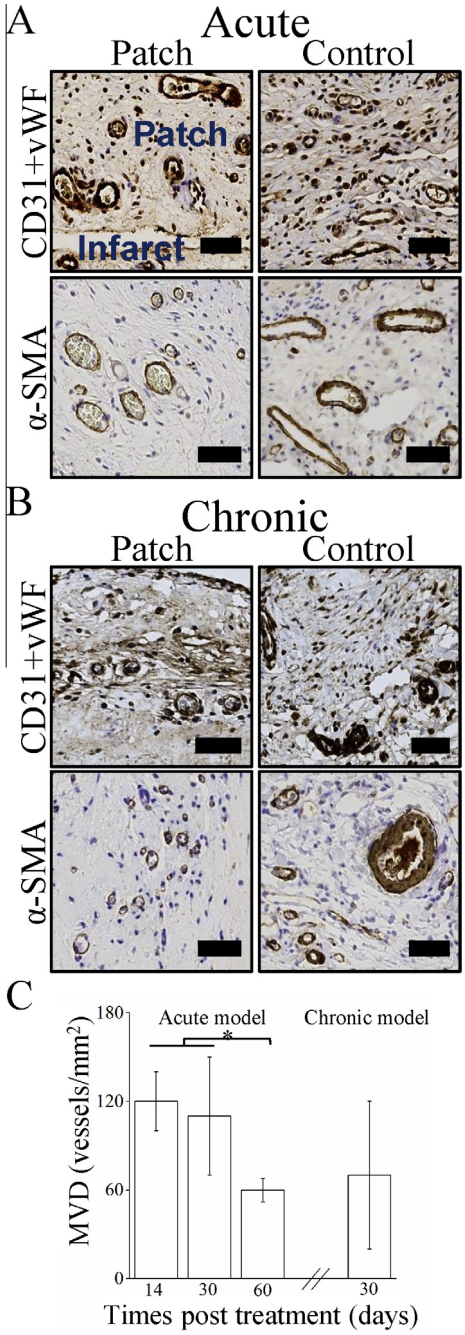

Fig. 6. pcECM-P vascularization. Representative IHC CD31 + vWF and α-SMA stains for blood vessels endothelium and smooth muscle cell, respectively, within the pcECM-P explants of acute (A) and chronic (B) MI models 30 days post treatment. Mean vessel density (MVD) quantifications (mean ± SD of n = 6 animals per time point) for 14, 30 and 60 (acute) and 30 (chronic) days post treatment (B). Scale bars: 50 μm. *Statistical significance indicator ($p < 0.05$).

results are *model-independent*, we conclude that pcECM-P efficacy involves, beyond the established mechanical support, an active biological mechanism, which is at least partly mediated at the cellular level by recruited progenitors that differentiate to CM-like cells and restore CF.

Chemoattraction to ECM natural degradation byproducts, termed 'matrikines' or 'bioactive matricryptic peptides', constitute a generally accepted mechanism of ECM bioactivity—inducing inflammation, angiogenesis, wound healing and regeneration [34,35]. The ability of decellularized ECM to induce a host regenerative response, according to this general mechanism, is dependent on the recruitment of tissue specific progenitor cells, as previously demonstrated, albeit for non-cardiac derived ECMs and other disease models [31,36,37]. Bioactive matrikine release occurs by various ECM remodeling enzymes (e.g., MMPs [38]), such as secreted by macrophages and fibroblasts. Such enzyme expression was previously also reported for our pcECM [20].

In particular, the major role of macrophages in both infarct healing [39] and ECM degradation and remodeling was highlighted [31,37]. It was suggested that early induction of an M2 macrophage 'regulatory' phenotype versus an M1 'activated' phenotype and

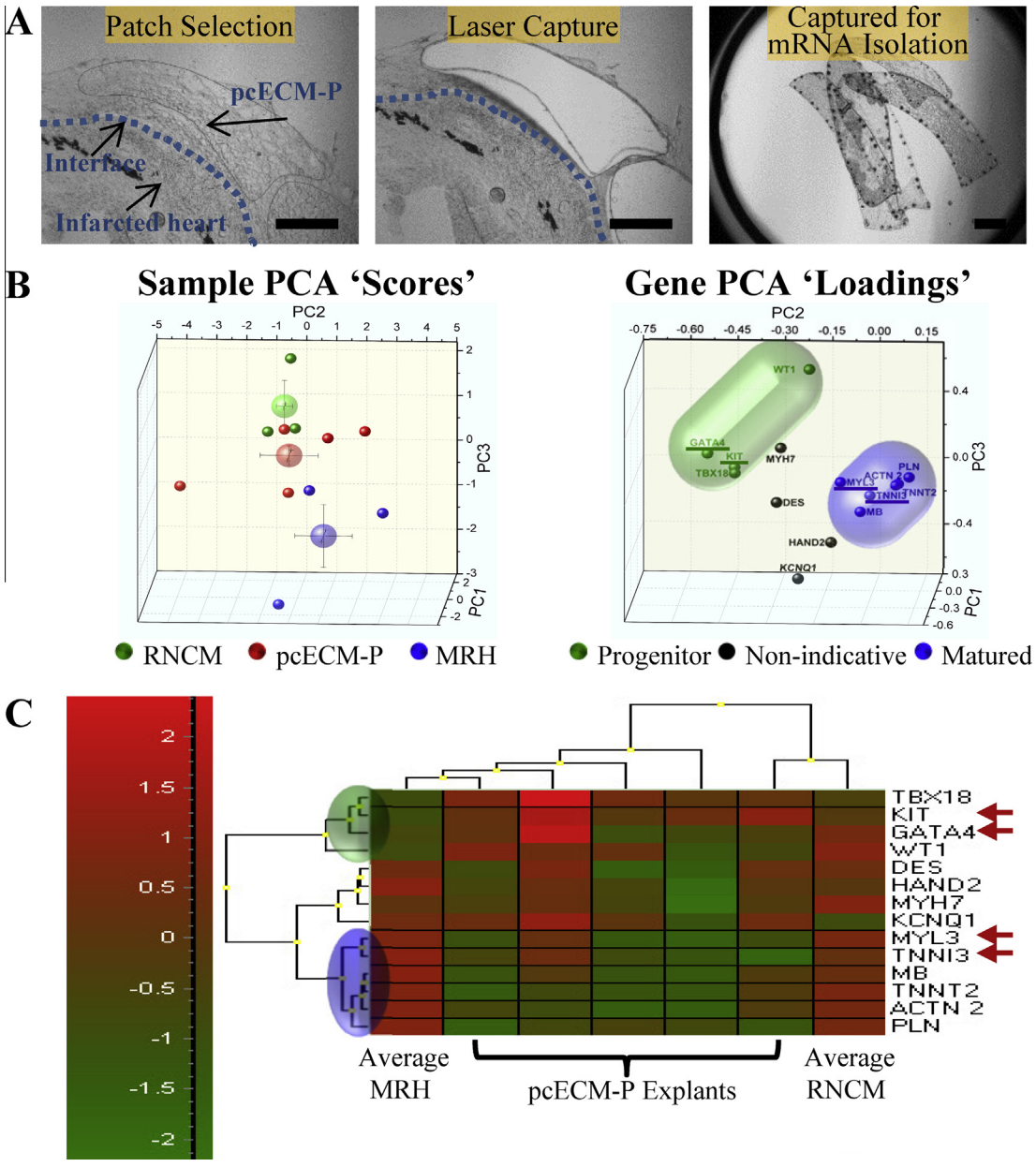

Fig. 7. Expression of cardiomyocyte (CM) progenitor and maturation markers in pcECM-P recruited host cells. Representative images (out of n = 5 animals) of patch cross-sectional regions are shown prior to and following LCM (A). Patch margins are larger when nearing the infarct border zone to avoid 'contaminating' mRNA from the infarct/heart tissue. PCA showing the sample 'scores' and gene 'loadings' 30 days post implantation (B). PcECM-P recruited cells are compared to two positive control groups: Rat neonatal CM (RNCM) and mature rat heart (MRH) biopsies'. Small spheres indicate single sample scores (mean ± SD); bigger spheres indicate the average and standard error for each sample group (B, left panel). 'Progenitor' (shaded in green) vs. 'mature' (shaded in blue) phenotype clusters are shown based on both relative PCA gene loadings (B, right panel) and on independent Ward's algorithm and absolute Pearson's correlation analyses represented in log(2) auto-scaled expression 'heat-map' (C). While all genes were positively expressed in all samples, their relative expression heat-map (low in green, and high in red) positions the pcECM-P samples in-between the average RNCM and MRH phenotypes. Two genes in each cluster were chosen for subsequent analyses at the protein level (B, underlined and C, arrows). Scale bars: 500 μm.

their ratio can serve as markers of bioinductive ECM based substances [31]. Quantification of M2 over M1 macrophage density ratios within the patch increased by almost sixfold from day 14 to the day 60 time-point, indicating a constructive reaction kinetics by the host immunity. Moreover, a similar ratio measured in both the acute and chronic models 30 days post implantation validates the assumption that the quantified effect is patch dependent and not animal model related. Indeed, this ratio correlates well to pathological scoring of a wide range of commercially available ECM materials. High scores (~9–13) reflected induction of a regenerative response and implant integration as opposed to lower scores indicating scar tissue formation, encapsulation or rejection [31]. Based on double-blinded evaluation and using the same scale, our pcECM-P yielded a score of 13 ± 1, portraying the pcECM as a strong bioinducing material, as also supported by our mRNA and protein level analyses.

mRNA analyses revealed that the recruited cell gene expression showed intermediate profile between two major gene clusters—'neonatal/progenitor' and 'mature native heart tissue'—possibly due to cell maturation process, yielding a 'transitional' gene expression pattern 30 days post implantation. GATA4 and MYLC, each belonging to a different cluster, were chosen as representative markers for protein level analyses, displaying co-localization as indicated by double positive cells. Both markers, but not others

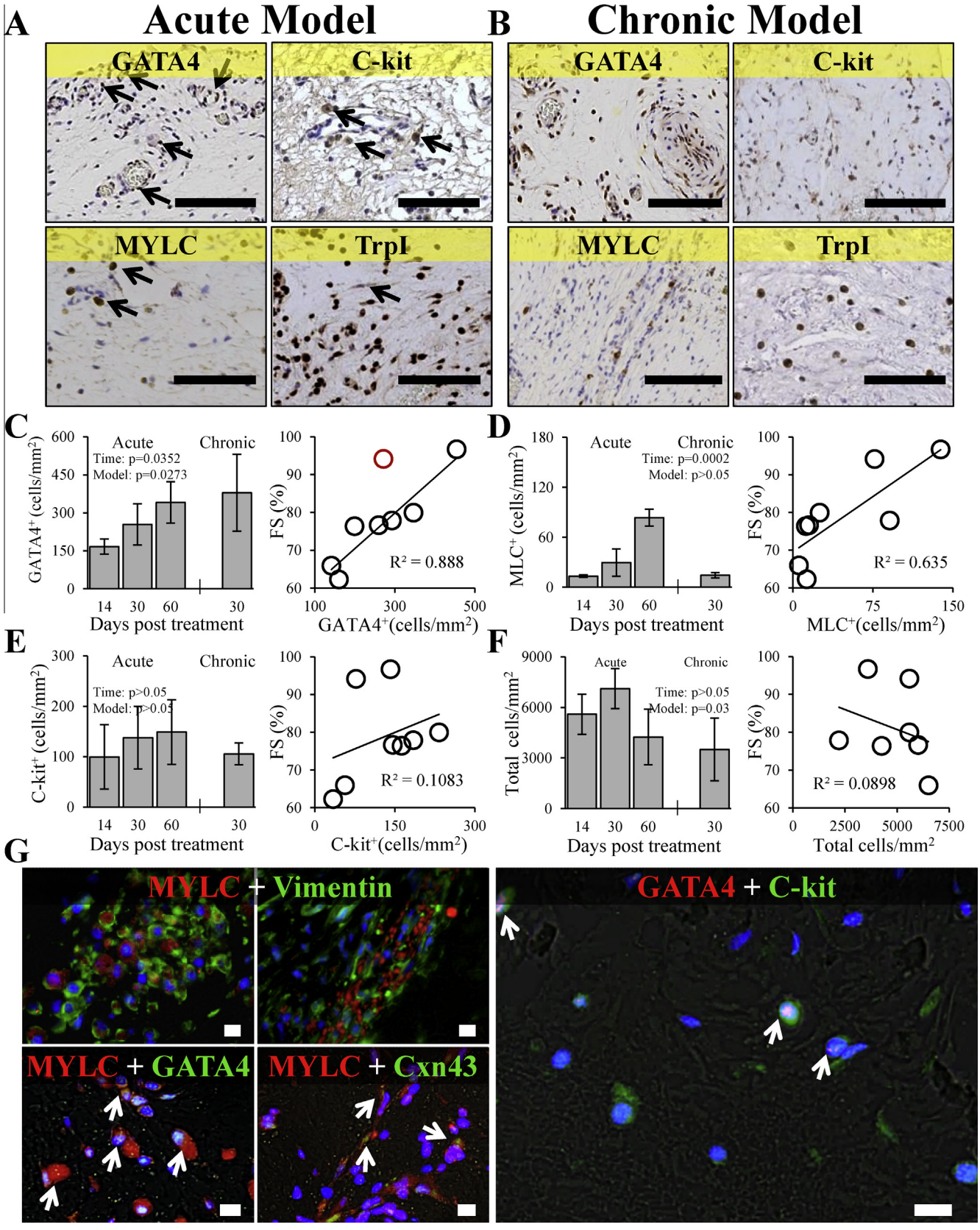

Fig. 8. Recruited progenitor and muscle cell density increases through time as cells self-organize in muscle 'fiber-like' structures. Representative IHC stains for GATA4, c-kit, MYLC, and TrpI expressed in explanted pcECM-Ps 30 days post implantation in acute (A) and chronic (B) models (brown, positive stains; blue, nuclei counterstaining). Image analyses quantifications per time and model of positive cell densities for GATA4, MYLC and c-kit (C-E, Left, respectively; n ⩾ 3 animals per time-point and group), and their respective linear regression correlation to functional improvement (FS, as representative; excluded outliers appear in red, C-E, Right). Total patch cell densities (F, Left) and total cell counts' lack of correlation (F, Right) are shown as control. Representative images (60x) of IF double stains (red and green as indicated), counter-stained with DAPI (blue) and overlaid on the bright-field (gray) image of the ECM fibers of pcECM-Ps' cross-section, 30 days post implantation (G). Co-expression is indicated by white arrows. Scale bars: (A and B) – 100 μm. (G) – 10 μm.

(e.g., c-kit, trpI and total cell counts), displayed a time-dependent increase in infiltration, which correlated to improved ventricular contractility. Particularly, the kinetic profile of their density ratio within the patch suggests that GATA4 expression precedes that of MYLC. Supporting this notion is the recent report showing that GATA4 up-regulates the expression of cardiac specific MYLC [40]. We, therefore, suggest that a differentiation process, in which GATA4$^+$ cells start expressing CM-specific MYLC with increasing frequency through time, occurs. This process highlights the importance of these two specific cell types/markers in a biological regenerative process transpiring following implantation.

GATA4 up-regulation was previously shown to enhance secretion of paracrine factors (e.g., IGF), which extended survival and contractility of neighboring CMs [41], endogenous cardiac stem cells and early committed cells [5], hence suggesting GATA4 biologically active role in cardiac regeneration. These mechanisms are in line with our findings in which GATA4$^+$ cell infiltration continues to rise throughout the experimental timeline and correlate to functional improvement. Interestingly, documented GATA4 expression in untreated infarcted rat heart was shown to peak two weeks after infarction and return to baseline levels after one month [42]. Conversely, in our study, the measured density of GATA4$^+$ cells within the pcECM-P continued to rise without indication of plateauing, suggesting that the regenerative process was still on-going even 60 days post implantation. Concomitantly, our histological evaluation suggests that *de novo* self-assembled 'muscle-like fibers' are being formed, comprising CM-like cells (MYLC$^+$ cells, sometimes also partially striated), ensheathed with supporting fibroblsats and forming gap–junctions (connexin43) with neighboring cells. These recruited CM-like (MYLC$^+$) cells may directly contribute to improved localized regional contractility, as previously suggested for urinary bladder matrix (UBM) in a cardiac muscle defect model [43]. A similar phenomenon was also documented for skeletal muscle tissues treated with decellularized matrix in a volumetric muscle loss model [44].

5. Conclusions

Our results point to a complicated regenerative process initiated and regulated by a cross-talk between pcECM, the host innate immune system and the cardiac resident progenitor/satellite cells. As an initial reaction, macrophages recognize pcECM as an acceptable and biocompatible material. This recognition translates into a constructive remodeling process in which angiogenesis likely occurs—through canonical inflammation mechanisms. During this process, some mild degradation of the pcECM material attracts cardiac progenitors such as GATA4$^+$ cells. As long as the mild degradation process occurs, chemoattraction is retained, which may explain the linear rate of progenitor cell infiltration throughout the experimental time line evaluated. The infiltrated GATA4$^+$ progenitor cells biologically contribute through paracrine signaling—improving CM salvage in the infarcted area. Subsequently, some of the GATA4$^+$ cells differentiated to (MYLC$^+$), though the possibility of parallel recruitment of both cell types into the patch cannot be entirely ruled out. These myocytes self-organize to muscle 'fiber-like' patterns, which are gap–junctional coupled in support of the underlying infarcts. Of note is that this suggested mechanism can regenerate and restore CF even after scar tissue has already formed, which to the best of our knowledge, has not been reported before.

Funding and disclosures

This work was supported by the Israeli Science Foundation (ISF Grant No. 1563/10, Jerusalem, Israel); the Randy L. & Melvin R. Berlin Family Research Center for Regenerative Medicine (Haifa, Israel); and the Singapore National Research Foundation (NRF) under the CREATE program: The Regenerative Medicine Initiative in Cardiac Restoration Therapy Research (Singapore). The authors have no additional conflict of interest to disclose.

Acknowledgments

The authors gratefully acknowledge the assistance of Mr. Hanumakumar Bogireddi for his share in qPCR data acquisition and the assistance of the Advanced Molecular Pathology Laboratory (AMPL) at the Agency for Science Technology and Research (A*Star) for their histopathological support.

Appendix A. Supplementary data

Supplementary data associated with this article can be found, in the online version, at http://dx.doi.org/10.1016/j.actbio.2016.08.031.

References

[1] L. Ye, W.H. Zimmermann, D.J. Garry, J. Zhang, Patching the heart: cardiac repair from within and outside, Circ. Res. 113 (2013) 922–932.
[2] M. Radisic, K.L. Christman, Materials science and tissue engineering: repairing the heart, Mayo Clin. Proc. 88 (2013) 884–898.
[3] U. Sarig, M. Machluf, Engineering cell platforms for myocardial regeneration, Expert Opin. Biol. Ther. 11 (2011) 1055–1077.
[4] M. Arnal-Pastor, J. Chachques, M.M. Pradas, A. Vallés-Lluch, Biomaterials for cardiac tissue engineering, in: P.J.A. Andrades (Ed.), Regenerative Medicine and Tissue Engineering: InTech, 2013, pp. 275–303.
[5] K. Urbanek, M. Rota, S. Cascapera, C. Bearzi, A. Nascimbene, A. De Angelis, T. Hosoda, S. Chimenti, M. Baker, F. Limana, Cardiac stem cells possess growth factor-receptor systems that after activation regenerate the infarcted myocardium, improving ventricular function and long-term survival, Circ. Res. 97 (2005) 663–673.
[6] S. Vandervelde, M.J. van Luyn, R.A. Tio, M.C. Harmsen, Signaling factors in stem cell-mediated repair of infarcted myocardium, J. Mol. Cell. Cardiol. 39 (2005) 363–376.
[7] K.A. Kyburz, K.S. Anseth, Synthetic mimics of the extracellular matrix: how simple is complex enough?, Ann Biomed. Eng. 43 (2015) 489–500.
[8] S.F. Badylak, D.J. Weiss, A. Caplan, P. Macchiarini, Engineered whole organs and complex tissues, Lancet 379 (2012) 943–952.
[9] L. Song, S.V. Murphy, B. Yang, Y. Xu, Y. Zhang, A. Atala, Bladder acellular matrix and its application in bladder augmentation, Tissue Eng. Part B Rev. 20 (2014) 163–172.
[10] K.A. Robinson, J. Li, M. Mathison, A. Redkar, J. Cui, N.A. Chronos, R.G. Matheny, S.F. Badylak, Extracellular matrix scaffold for cardiac repair, Circulation 112 (2005) I135–I143.
[11] P.V. Kochupura, E.U. Azeloglu, D.J. Kelly, S.V. Doronin, S.F. Badylak, I.B. Krukenkamp, I.S. Cohen, G.R. Gaudette, Tissue-engineered myocardial patch derived from extracellular matrix provides regional mechanical function, Circulation 112 (2005) I144–I149.
[12] H.J. Wei, C.H. Chen, W.Y. Lee, I. Chiu, S.M. Hwang, W.W. Lin, C.C. Huang, Y.C. Yeh, Y. Chang, H.W. Sung, Bioengineered cardiac patch constructed from multilayered mesenchymal stem cells for myocardial repair, Biomaterials 29 (2008) 3547–3556.
[13] H.E. Mewhort, J.D. Turnbull, H.C. Meijndert, J.M. Ngu, P.W. Fedak, Epicardial infarct repair with basic fibroblast growth factor-enhanced CorMatrix-ECM biomaterial attenuates postischemic cardiac remodeling, J. Thorac. Cardiovasc. Surg. 147 (2014) 1650–1659.
[14] S. Badylak, J. Obermiller, L. Geddes, R. Matheny, Extracellular matrix for myocardial repair, Heart Surg. Forum 6 (2003) E20–E26.
[15] S.F. Badylak, D. Taylor, K. Uygun, Whole-organ tissue engineering: decellularization and recellularization of three-dimensional matrix scaffolds, Annu. Rev. Biomed. Eng. (2011).
[16] H.C. Ott, T.S. Matthiesen, S.K. Goh, L.D. Black, S.M. Kren, T.I. Netoff, D.A. Taylor, Perfusion-decellularized matrix: using nature's platform to engineer a bioartificial heart, Nat. Med. 14 (2008) 213–221.
[17] P. Akhyari, H. Aubin, P. Gwanmesia, M. Barth, S. Hoffmann, J. Huelsmann, K.H. Preuss, A. Lichtenberg, The quest for an optimized protocol for whole heart decellularization: a comparison of three popular and a novel decellularization technique and their diverse effects on crucial extracellular matrix qualities, Tissue Eng. Part C Methods (2011).
[18] J.M. Singelyn, J.A. DeQuach, S.B. Seif-Naraghi, R.B. Littlefield, P.J. Schup-Magoffin, K.L. Christman, Naturally derived myocardial matrix as an injectable scaffold for cardiac tissue engineering, Biomaterials 30 (2009) 5409–5416.

[19] J.M. Wainwright, C.A. Czajka, U.B. Patel, D.O. Freytes, K. Tobita, T.W. Gilbert, S. F. Badylak, Preparation of cardiac extracellular matrix from an intact porcine heart, Tissue Eng. Part C Methods 16 (2010) 525–532.
[20] Y. Eitan, U. Sarig, N. Dahan, M. Machluf, Acellular cardiac extracellular matrix as a scaffold for tissue engineering: in vitro cell support, remodeling, and biocompatibility, Tissue Eng. Part C Methods 16 (2010) 671–683.
[21] B. Wang, A. Borazjani, M. Tahai, A.L. Curry, D.T. Simionescu, J. Guan, F. To, S.H. Elder, J. Liao, Fabrication of cardiac patch with decellularized porcine myocardial scaffold and bone marrow mononuclear cells, J. Biomed. Mater. Res. A 94 (2010) 1100–1110.
[22] U. Sarig, G.C. Au-Yeung, Y. Wang, T. Bronshtein, N. Dahan, F.Y. Boey, S.S. Venkatraman, M. Machluf, Thick acellular heart extracellular matrix with inherent vasculature: a potential platform for myocardial tissue regeneration, Tissue Eng. Part A 18 (2012) 2125–2137.
[23] A.F. Godier-Furnemont, T.P. Martens, M.S. Koeckert, L. Wan, J. Parks, K. Arai, G. Zhang, B. Hudson, S. Homma, G. Vunjak-Novakovic, Composite scaffold provides a cell delivery platform for cardiovascular repair, Proc. Natl. Acad. Sci. U.S.A. 108 (2011) 7974–7979.
[24] T.D. Johnson, J.A. DeQuach, R. Gaetani, J. Ungerleider, D. Elhag, V. Nigam, A. Behfar, K.L. Christman, Human versus porcine tissue sourcing for an injectable myocardial matrix hydrogel, Biomater. Sci. (2014).
[25] U. Sarig, E.B. Nguyen, Y. Wang, S. Ting, T. Bronshtein, H. Sarig, N. Dahan, M. Gvirtz, S. Reuveny, S.K. Oh, T. Scheper, Y.C. Boey, S.S. Venkatraman, M. Machluf, Pushing the envelope in tissue engineering: ex vivo production of thick vascularized cardiac extracellular matrix constructs, Tissue Eng. Part A 21 (2015) 1507–1519.
[26] T. Bronshtein, G.C. Au-Yeung, U. Sarig, E.B. Nguyen, P.S. Mhaisalkar, F.Y. Boey, S.S. Venkatraman, M. Machluf, A mathematical model for analyzing the elasticity, viscosity, and failure of soft tissue: comparison of native and decellularized porcine cardiac extracellular matrix for tissue engineering, Tissue Eng. Part. C Methods 19 (2013) 620–630.
[27] S.E. Litwin, S.E. Katz, J.P. Morgan, P.S. Douglas, Serial echocardiographic assessment of left ventricular geometry and function after large myocardial infarction in the rat, Circulation 89 (1994) 345–354.
[28] E.E. Morgan, M.D. Faulx, T.A. McElfresh, T.A. Kung, M.S. Zawaneh, W.C. Stanley, M.P. Chandler, B.D. Hoit, Validation of echocardiographic methods for assessing left ventricular dysfunction in rats with myocardial infarction, Am. J. Physiol. Heart Circ. Physiol. 287 (2004) H2049–H2053.
[29] R.M. Lang, M. Bierig, R.B. Devereux, F.A. Flachskampf, E. Foster, P.A. Pellikka, M. H. Picard, M.J. Roman, J. Seward, J. Shanewise, Recommendations for chamber quantification, Eur. J. Echocardiography 7 (2006) 79–108.
[30] P. Pacher, T. Nagayama, P. Mukhopadhyay, S. Batkai, D.A. Kass, Measurement of cardiac function using pressure-volume conductance catheter technique in mice and rats, Nat. Protoc. 3 (2008) 1422–1434.
[31] B.N. Brown, R. Londono, S. Tottey, L. Zhang, K.A. Kukla, M.T. Wolf, K.A. Daly, J.E. Reing, S.F. Badylak, Macrophage phenotype as a predictor of constructive remodeling following the implantation of biologically derived surgical mesh materials, Acta Biomater. 8 (2012) 978–987.
[32] E.B. Prophet, B. Mills, J.B. Arrington, L.H. Sobin, Laboratory methods in histotechnology: American registry of pathology Washington, DC, 1992.
[33] M. Plotkin, S.R. Vaibavi, A.J. Rufaihah, V. Nithya, J. Wang, Y. Shachaf, T. Kofidis, D. Seliktar, The effect of matrix stiffness of injectable hydrogels on the preservation of cardiac function after a heart attack, Biomaterials 35 (2014) 1429–1438.
[34] F.X. Maquart, G. Bellon, S. Pasco, J.C. Monboisse, Matrikines in the regulation of extracellular matrix degradation, Biochimie 87 (2005) 353–360.
[35] S. Ricard-Blum, R. Salza, Matricryptins and matrikines: biologically active fragments of the extracellular matrix, Exp. Dermatol. 23 (2014) 457–463.
[36] A.J. Beattie, T.W. Gilbert, J.P. Guyot, A.J. Yates, S.F. Badylak, Chemoattraction of progenitor cells by remodeling extracellular matrix scaffolds, Tissue Eng. Part A 15 (2008) 1119–1125.
[37] J.E. Valentin, A.M. Stewart-Akers, T.W. Gilbert, S.F. Badylak, Macrophage participation in the degradation and remodeling of extracellular matrix scaffolds, Tissue Eng. Part A 15 (2009) 1687–1694.
[38] J.M. Wells, A. Gaggar, J.E. Blalock, MMP generated matrikines, J. Int. Soc. Matrix Biol. 44–46 (2015) 122–129.
[39] T. Ben-Mordechai, R. Holbova, N. Landa-Rouben, T. Harel-Adar, M.S. Feinberg, I. A. Elrahman, G. Blum, F.H. Epstein, Z. Silman, S. Cohen, Macrophage subpopulations are essential for infarct repair with and without stem cell therapy, J. Am. Coll. Cardiol. 62 (2013) 1890–1901.
[40] A. Yamak, B.V. Latinkić, R. Dali, R. Temsah, M. Nemer, Cyclin D2 is a GATA4 cofactor in cardiogenesis, Proc. Natl. Acad. Sci. U.S.A. 111 (2014) 1415–1420.
[41] N. Kawaguchi, A.J. Smith, C.D. Waring, M.K. Hasan, S. Miyamoto, R. Matsuoka, G.M. Ellison, C-kitpos GATA-4 high rat cardiac stem cells foster adult cardiomyocyte survival through IGF-1 paracrine signalling, PLoS ONE 5 (2010) e14297.
[42] J. Rysa, O. Tenhunen, R. Serpi, Y. Soini, M. Nemer, H. Leskinen, H. Ruskoaho, GATA-4 is an angiogenic survival factor of the infarcted heart, Circ. Heart Fail 3 (2010) 440–450.
[43] D.J. Kelly, A.B. Rosen, A.J. Schuldt, P.V. Kochupura, S.V. Doronin, I.A. Potapova, E.U. Azeloglu, S.F. Badylak, P.R. Brink, I.S. Cohen, Increased myocyte content and mechanical function within a tissue-engineered myocardial patch following implantation, Tissue Eng. Part A 15 (2009) 2189–2201.
[44] B.M. Sicari, J.P. Rubin, C.L. Dearth, M.T. Wolf, F. Ambrosio, M. Boninger, N.J. Turner, D.J. Weber, T.W. Simpson, A. Wyse, E.H. Brown, J.L. Dziki, L.E. Fisher, S. Brown, S.F. Badylak, An acellular biologic scaffold promotes skeletal muscle formation in mice and humans with volumetric muscle loss, Sci. Transl. Med. 6 (2014) 234–258.